J Solid State Electrochem (2011) 15:153–160
DOI 10.1007/s10008-010-1080-2

ORIGINAL PAPER

Silver nanoparticles embedded phosphomolybdate–polyaniline hybrid electrode for electrocatalytic reduction of H_2O_2

Arumugam Manivel · Sambandam Anandan

Received: 12 January 2010 / Revised: 2 March 2010 / Accepted: 15 April 2010 / Published online: 7 May 2010

Abstract Hybrid silver/phosphophomolybdate/polyaniline (Ag/PMo12/PAni) was obtained through one pot synthesis, and then, it was successfully fabricated on the glassy carbon electrode by simple casting method for electrocatalytic reduction of hydrogen peroxide (H_2O_2). The cyclic voltammetric studies of the Ag/PMo12/PAni hybrid electrode suggest that the electronic properties of the phosphomolybdate are retained even after the formation of hybrid material and in addition effectively electro-catalyzing the reduction of H_2O_2 with a less negative over potential. The Ag/PMo12/PAni-modified electrode showed the lowest detection limit (750 nM) for H_2O_2 reduction among the hybrid-modified electrodes already reported with a sensitivity of 4.398 nA μM^{-1}. The prepared hybrid material was well characterized by using UV, XRD and TEM analysis.

Keywords Hybrid materials · Polyaniline · Phosphomolybdate · Silver nanoparticles · Modified electrode · H_2O_2 sensor

Introduction

Design, fabrication and application of novel electrochemical sensors have been a topic of research in recent years [1, 2]. For this aspect, modification of electrodes with suitable functionalities is an ongoing task among researchers world-wide because of its ability to improve the electron transfer rate from substrates to the electrode [3, 4]. In this topic of research, modification of electrode surfaces with heteropolyacids (HPAs) has received much attention [5, 6] owing to their attractive electronic and molecular properties, which results in novel applications in catalysis [7], materials science [8] and energy storage devices [9, 10] etc. Several immobilization techniques (adsorption [11, 12], electrochemical deposition [13, 14], layer-by-layer deposition [15–18], entrapment into sol-gel matrices [19, 20], organo-ceramic materials [21], silica gel [22], ordered meso-porous carbon [23], carbon nanotubes [24] etc.) have been exploited in literature to anchor HPAs at the electrodes surfaces. However, the high solubility of heteropolyacids in aqueous media limits the stability of those modified electrodes, as it leads to leaching of heteropolyanion from the electrode surface and to the consequent drop of their electrochemical features [25, 26]. However, entrapping HPA into conducting polymer matrix leads to the fabrication of molecular hybrid materials which minimizes the leaching of HPA due to its interactions with the polymer matrix and the poor solubility of the conducting polymer in water [27] and in addition, inorganic clusters (HPA) keep their integrity and activity while benefiting from the conducting properties and polymeric nature of the hybrid structure [9, 28]. Further incorporation of metal nanoparticles into the inorganic–organic hybrid materials offers enhanced performance due to the increase in conductivity and surface area [29]. This has been evidenced from the results published by Kulesza et al. [15, 17], who observed higher electrocatalytic activity using polymer-based hybrid films with gold and platinum nanoparticles compared with bare electrodes. In this regard, we made an attempt to fabricate modified electrodes with metal-incorporated inorganic–organic hybrid material for electrocatalytic reduction of H_2O_2, i.e. silver-incorporated phosphomolymdate–polyaniline (Ag/PMo12/PAni). Although some attempts have

A. Manivel · S. Anandan (✉)
Nanomaterials and Solar Energy Conversion Lab,
Department of Chemistry, National Institute of Technology,
Trichy 620 015, India
e-mail: sanand99@yahoo.com
e-mail: sanand@nitt.edu

been done in the preparation of hybrid materials with metal nanoparticles [29], the electrocatalytic application via simple fabrication route are still open for investigation. Hence in the present paper, we developed a facile method to fabricate a metal-incorporated inorganic–organic composite-modified glassy carbon (GC); its electrochemical properties and its electrocatalytic activity towards the H_2O_2 reduction.

Experimental

Aniline from SRL chemicals was distilled under vacuum prior to use. Phosphomolybdic acid ($H_3PMo_{12}O_{40}$) was purchased from Aldrich and used without further purification. $AgNO_3$, KCl and $K_3[Fe(CN)_6]$ were obtained from E-Merck. Unless otherwise specified, all the reagents used were of analytical grade and the solutions were prepared using millipore water.

Surface morphology, particle size and the various contours of the hybrid materials were analyzed by XRD (measured using Rigaku diffractometer, Cu-Kα radiation, Japan) and Transmission electron microscopy (recorded using TECNAI G^2 model), respectively. UV-vis spectra of the samples were recorded using a T90+ double beam UV-visible Spectrophotometer purchased from PG-Instruments, UK. The electrochemical experiments were carried out using CHI650C model CH Instruments, USA.

A conventional three-electrode assembly was used for cyclic voltammetric measurements. A GC electrode and platinum wire procured from CH Instruments (USA) were employed as the working electrode and counter electrode, respectively. Ag/AgCl electrode purchased from BASi (USA) was used as the reference electrode. The glassy carbon electrode (GCE) was conditioned through a polishing and cleaning procedure. The polishing was carried out with 1.0, 0.3, 0.05 μm grain size alumina powder successively in a micro-cloth polishing pad. Then the electrode was washed with Milli-Q water and finally cleaned in an ultrasonic bath for 5 min and dried in air. Electrochemical pre-treatment has been performed according to the known procedure as follows: That is electrodes were potentiodynamically cycled between anodic and sufficient cathodic potentials (−0.5 to 1.3 V) in acidic 0.5 M H_2SO_4 media at slow sweep rates (5 mVs^{-1}) for 15–30 min. Such pre-treatment generally gave reproducible results for $Fe(CN)_6^{3-/4-}$ redox couple even after 2–3 h. Such electrodes were called in general as standardized electrode. The solutions were thoroughly degassed by slow bubbling (≈10 ml min^{-1}) of high pure nitrogen for at least 15 min prior to measurements. For the steady-state amperometry experiments, a magnetic stirrer was used to stir the solution. The background current was allowed to decay to a constant value before adding the analyte. All the experiments were carried out at room temperature (25±2 °C).

Synthesis of hybrid Ag/PMo12/PAni

About 0.7 mM aqueous solution of phosphomolybdic acid was directly added to 0.5 mM of freshly distilled aniline, in order to form the phosphomolybdate anion (heteropolyblue) and polyaniline(PAni) by one electron transfer processes (redox phenomena), which is identified by immediate change in initial color from yellow to deep blue. The mixture was stirred for 15 min under inert atmosphere. To this solution, about 0.1 mM of aqueous $AgNO_3$ solution was added and the solution was kept irradiated for 2 h using UV light source (15 W UV lamp; λ_{max}=355 nm) with continuous stirring. After irradiation, the solution was kept undisturbed for 2 h to get a solid precipitate. Then the solid precipitate was filtered and washed several times with copious amount of double distilled water to remove any unreacted PMo12 and then with methanol to remove any oligomeric aniline. Finally, the precipitate was dried in vaccum at 60 °C for electrocatalytic studies.

Fabrication of the Ag/PMo12/PAni-modified electrode

A 5 mg of the Ag/PMo12/PAni hybrid material was mixed with 0.5 ml of acetonitrile (CH_3CN) solvent and ultrasonicated for 15 min in order to get a homogenized colloidal solution. About 3 μL of homogenized colloidal solution was casted on a standardized glassy carbon electrode and dried under normal atmospheric conditions for 2 h. Then the electrode was throughly washed with distilled water and 1.0 M sulphuric acid. Electrochemical pretreatment was carried out for the above-modified electrode in 1.0 M H_2SO_4 by continuous potential sweep (50 mVs^{-1}) between +0.8 V to −0.1 V until the modified electrode gives stable voltammogram. Electrodes with higher microdrop volumes (5, 7, 9 μL) were also fabricated and tested, however the observed cyclic voltammogram for modified electrode with 3 μLwas the best without any surface defects.

Results and discussion

Characterization of hybrid Ag/PMo12/PAni

The formation of Ag/PMo12/PAni hybrid material could be explained with the help of UV-visible spectra. It is well known that the PMo12 will show two absorbance bands around 260 and 318 nm owing to O→Mo charge transfer transitions (Fig. 1a). Upon adding the aniline monomer into PMo12 solution, we could see the characteristic change in

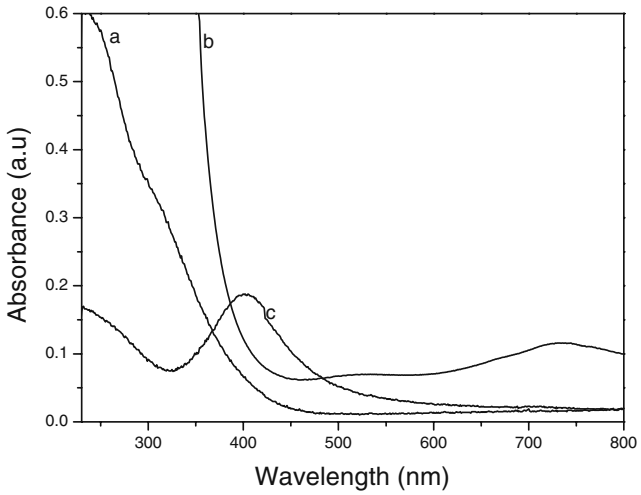

Fig. 1 UV-visible absorbance spectra of (**a**). PMo12, (**b**). PMo12/PAni and (**c**). Ag/PMo12/PAni

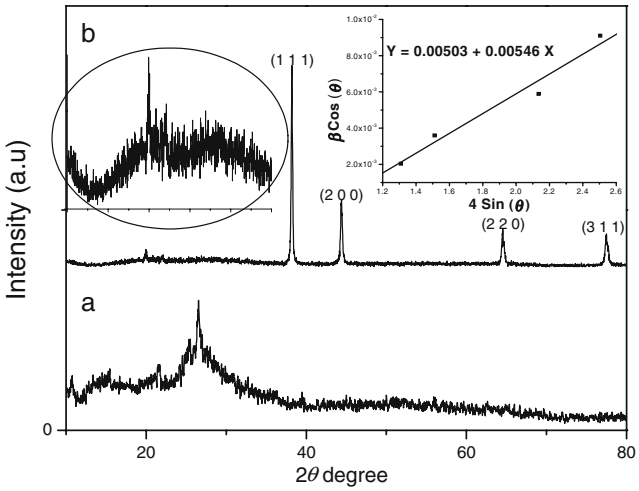

Fig. 2 X-ray diffraction patterns of (**a**). PMo12/PAni and (**b**). Ag/PMo12/PAni. The inset shows the Williamson–Hall plot for the calculation of crystallite strain and size

the UV spectrum (Fig. 1b). It is worth noting that a new peak around 730 nm, which indicates the formation of one electron reduced phosphomolybdate anion (heteropolyblue) by oxidizing aniline monomer. The addition of silver nitrate to the above solution, results in the reduction of silver ions to metallic silver by one electron reduced phosphomolybdate anion and it returns back to its initial state (PMo12). The formation of silver nanoparticles is evident by a surface plasmon band around 400 nm (Fig. 1c). During these reduction processes, as formed PMo12 adsorb on the metallic surface provides kinetic stabilization through columbic repulsion and steric stabilization [15, 30, 31]. In addition, silver nanoparticles get embedded with cationic polyaniline matrix exhibit regular packing with offset aromatic–aromatic interaction led to compact structure as shown in Scheme 1, where the ratio of six aromatic ring per PMo12 molecule is ideal expected value [9, 10] and the reduced PMo12 is re-oxidized by the silver ion.

The phase identification for the prepared hybrid material was carried out using powder X-ray diffraction. The observed XRD pattern of Ag/PMo12/PAni hybrid material are more crystalline and shows four well resolved diffraction peaks (2θ) characteristic of silver (38.14°, 44.39°, 64.51° and 77.47° representing the Bragg's reflection planes (1 1 1), (2 0 0), (2 2 0) and (3 1 1), respectively) (Fig. 2a). For comparative purpose, XRD patterns of silver free sample (PMo12/PAni) are given in Fig. 2b which has been prepared according to the known procedure [32]. Diffraction peak at about 26.52° shows the characteristic formation of PAni which is clearly visible in the case of silver free PMo12/PAni hybrid material whereas the observed intensity of the peak was very low in the case of Ag/PMo12/PAni hybrid material (see inset expanded XRD figure). Reason for such low intensity is due to the presence of silver in Ag/PMo12/PAni hybrid material which modi-

Scheme 1 The pictorial representation of the hybrid Ag/PMo12/PAni

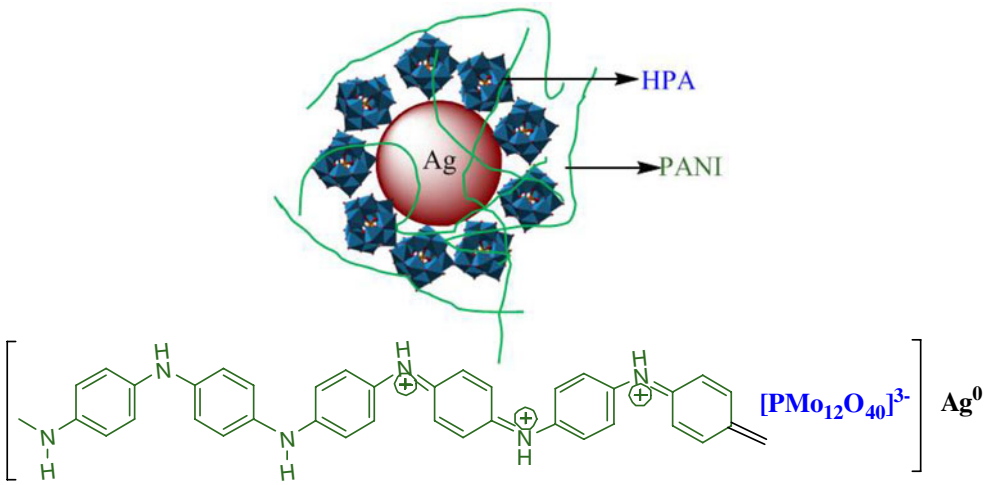

fied the relative ratio between the crystalline and amorphous structures. Further, no XRD diffraction patterns are noticed for bulk PMo12 crystallite phase indicates that the PMo12 are finely dispersed in the PAni matrix.

The presence of nanosized silver particles in the hybrid material induces lattice strain which contributes broadening of XRD peaks. However, the crystallite size and strain contributions to line broadening are independent of each other [33]. Hence, the total peak broadening is represented by sum of the crystallite size and strain contributions [33] and it is calculated from the X-ray diffraction pattern using Williamson–Hall equation as follows

$$\beta \cos\theta = \frac{K\lambda}{d} + 4\varepsilon \sin\theta$$

Where K is the shape factor which is 0.9 for uniform small-sized crystals, λ is wavelength of X-ray, θ is Bragg's angle, ε is the strain, d is average crystallite size and β is full-width half-maximum value. Plotting the value of $\beta \cos\theta$ vs 4sinθ (see inset of Fig. 2), the strain (5.46 10^{-3}) may be estimated from the slope of the line and the average crystallite size (27.5 nm) may be estimated from the intersection with the vertical axis.

The transmission electron microscopy (TEM) was employed to investigate the morphology and size of the silver nanoparticles in the hybrid materials. Figure 3a shows the representative transmission electron micrographic image of Ag/PMo12/PAni. The formed silver nanoparticles are polydisperse and of irregular morphology with the size ranging from 20 to 50 nm. Figure 3b shows the high resolution TEM image of one of the silver nanoparticles. The grey shadow present in the particles may be due the PMo12 layer coved on the silver nanoparticles. The observed selected area electron diffraction (SAED) pattern for the silver nanoparticles is shown in Fig. 3c. Thus, the TEM images provide further evidence for the presence of silver nanoparticles in the polymer hybrid matrix.

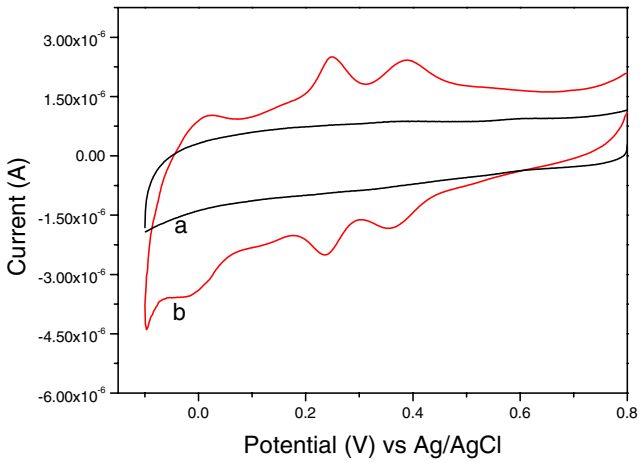

Fig. 4 Cyclic voltammogram of (**a**). Bare GC electrode and (**b**). Ag/PMo12/PAni-modified electrode in 1.0 M H_2SO_4. Sweep rate 50 mVs^{-1}

Cyclic voltammetric behaviour of Ag/PMo12/PAni-modified electrode

The cyclic voltammetric responses of Ag/PMo12/PAni-modified electrode has been investigated using 1.0 M sulphuric acid because, heteropolyacid is unstable in both neutral and basic solutions and undergoes sequence hydrolysis process [6]. Figure 4 shows the cyclic voltammograms of the bare GC electrode and Ag/PMo12/PAni-modified GC electrode in 1.0 M H_2SO_4 solution in the potential range of +0.8 V to −0.1 V at 50 mVs^{-1}. As can be seen, the voltammograms shows three set of characteristics peaks for PMo12 similar to that of the PMo12 monolayer electrode formed by adsorption [6], which suggests that no electronic structural changes have taken place in PMo12 even after formation of hybrid material. It means that the electrochemical processes of getting or losing protons of Ag/PMo12/PAni-modified electrode are consistent with the electrochemical behaviour of PMo12 anions in 1.0 M H_2SO_4 aqueous solution which maintains the charge neutrality and stability of the

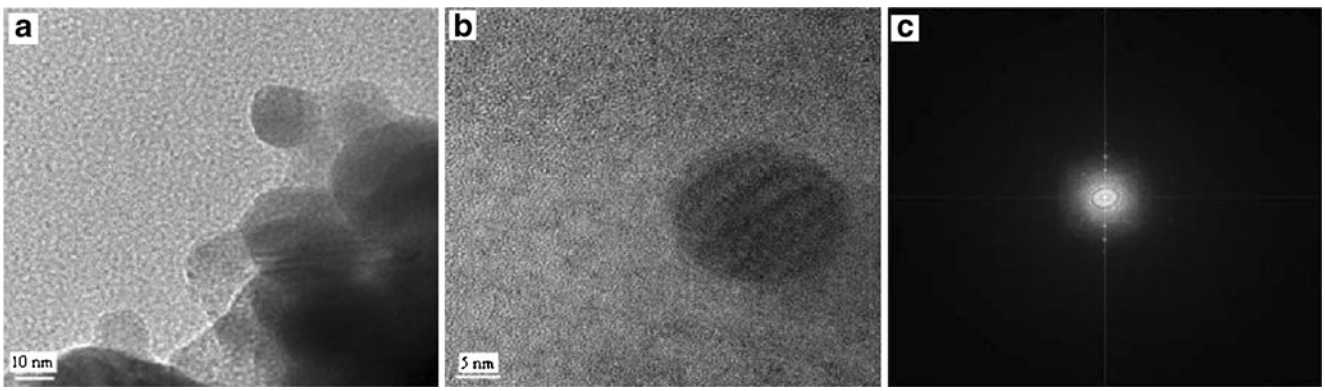

Fig. 3 TEM micrographic images of Ag/PMo12/PAni Ag/PMo12/PAni (**a**). Overview of a part of the hybrid (**b**). HRTEM of the Ag nanoparticle and (**c**, **d**). The SAED pattern of silver

electrode and hence the redox potentials depends on the pH of the medium. The redox reactions for such characteristic peaks are interepreted in terms of three consequetive two electron processes as described in the following Eqs. 1–3.

$$PMo_{12}O_{40}^{3-} + 2e^- + 2H^+ \rightleftarrows H_2PMo_{12}O_{40}^{3-} \quad (1)$$

$$H_2PMo_{12}O_{40}^{3-} + 2e^- + 2H^+ \rightleftarrows H_4PMo_{12}O_{40}^{3-} \quad (2)$$

$$H_4PMo_{12}O_{40}^{3-} + 2e^- + 2H^+ \rightleftarrows H_6PMo_{12}O_{40}^{3-} \quad (3)$$

The cyclic voltammogram of the hybrid Ag/PMo12/PAni-modified electrode at different scan rates has also been recorded and shown in Fig. 5. The first two redox potentials are independent of sweep rate and the third one is shifted towards less negative potential but the mean peak potential did not change on the whole. Both the anodic and cathodic peak currents of the voltammograms were linearly proportional to scan rate in the range of 20–640 mVs^{-1}. This indicates that the hybrid material contains uniformly dispersed PMo12 in the polymeric matrix and also the electrochemical process is surface controlled, ideally reversible and the exchange rate of the electrons are fast. A plot of peak current versus square root of scan rate gives a straight line passing through the origin indicates that the redox process is difussion controlled (inset of Fig. 5).

Electrocatalytic reduction of hydrogen peroxide

Due to electrochemical reversibility and higher electron transfer ability of Ag/PMo12/PAni hybrid-modified glassy carbon electrode, it may be used as a mediator to shuttle electron between electrodes and analyte molecules. This is because, reduced PMo12 are capable of delivering electrons to other species, thus serving as poweful electron reservoirs for multi-electron reduction [24]. Hence, we chose H_2O_2 as the substrate of analytical interest in our experiment to test the electrocatalytic activity of the Ag/PMo12/PAni hybrid electrode. Figure 6 shows typical cyclic voltammetric behaviour of Ag/PMo12/PAni-modified electrode towards electrocatalytic reduction of various concentrations of H_2O_2 (0.5–2 mM) in 1.0 M H_2SO_4 medium. The catalytic reduction current of hydrogen peroxide starts around 200 mV and an obvious catalytic reduction peak appears at the potential of 0.0 V. By increasing the concentration of H_2O_2 (0.5–2 mM), the cathodic peak current of the modified electrode is increased while its anodic peak current decreased. Thus, the observed catalytic current has linear relationship with the concentration of H_2O_2 with a correlation coeffecient of 0.9972 (see inset of Fig. 6). This infers that electrocatalytic reduction process takes place in the hybrid-modified electrode as shown schematically in Scheme 2.

Amperometric determination of H_2O_2

On the basis of the voltammetric results described above, it is possible to use the Ag/PMo12/PAni-modified GC electrode as an amperometric hydrogen peroxide sensor. The effect of applied potentials on the reduction of H_2O_2 at Ag/PMo12/PAni-modified electrode was determined by chronoamperometry. Figure 7 shows that the onset of the electrocatalytic reduction of H_2O_2 was observed around +200 mV and the steady-state current was increased when the applied potential was more negative. However, no increase in the catalytic current was observed when the applied potential is beyond 0.0 V. Hence, it is preferable to apply lower working potential to avoid or decrease the

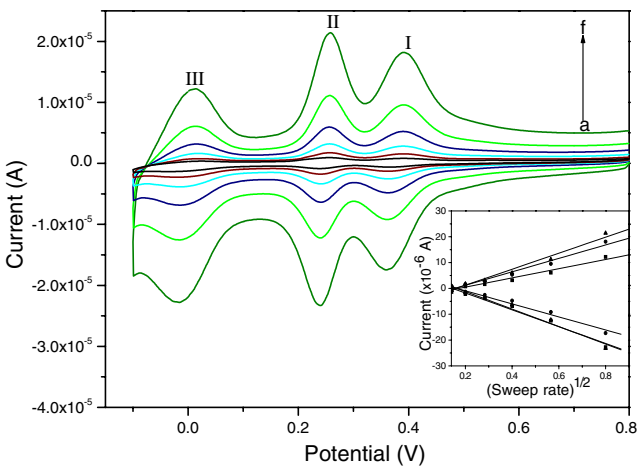

Fig. 5 Cyclic voltammograms obtained for Ag/PMo12/PAni-modified electrode in 1.0 M H_2SO_4 at different scan rates **a** 20, **b** 40, **c** 80, **d** 160, **e** 320 and **f** 640 mV s^{-1}. Inset plot shows the effect of square root of sweep rate on peak current

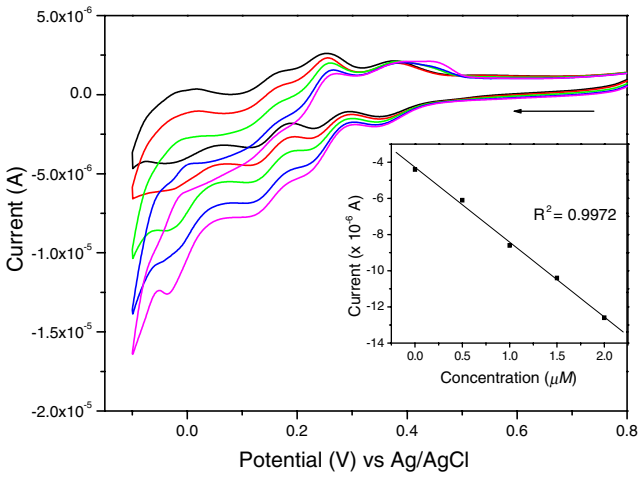

Fig. 6 Electrocatalytic reduction of hydrogen peroxide in Ag/PMo12/PAni modified electrode at different concentrations of H_2O_2. Concentration of H_2O_2=0, 0.5, 1, 1.5 and 2 mM, respectively. The inset shows the calibration plot of peak current versus concentration

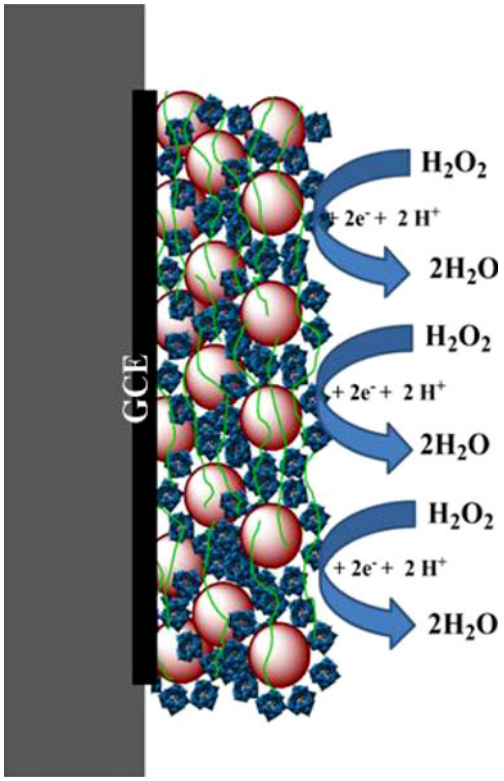

Scheme 2 The schematic representation of the electrocatalytic reduction of Ag/PMo12/PAni-modified electrode

interference. Since the sensor should have maximum sensitivity at 0.0 V, such potential was chosen for the amperometry experiments for determination of H_2O_2.

Amperometric *i–t* curve were recorded in Ag/PMo12/PAni-modified electrode under homogeneously stirred conditions at constant applied potential of 0.0 V in 1.0 M H_2SO_4 solution. As we can see in Fig. 8, during the successive addition of 2 μM H_2O_2 with a sample interval of 100 s, a well-defined response is observed. For each addition of H_2O_2 within a response time of less than 3 s, a sharp increase in the current was observed in negative direction. Thus, among the worked concentration range (2–20 μM) the response obtained increased linearly with increasing concentration of H_2O_2 (see inset of Fig. 8). The linear least square calibration curve over the above range had slope of 4.398 nA μM^{-1} (sensitivity) and a correlation coefficient of 0.9995. Owing to the fact that amperometry under stirred conditions has a much higher current sensitivity than cyclic voltammetry or chronoamperometry, which was used to estimate the lowest detection limit of H_2O_2 at an Ag/PMo12/PAni-modified electrode. According to the method mentioned in Ref. [34], the minimum distinguishable analytical signal, S_m, is taken as the sum of the mean blank signal, S_{bl}, plus a multiple 3 of the standard deviation of the blank, S_{bl}. That is, $S_m=S_{bl}+3s_{bl}$. In this experiment, 15 replicate measurements were performed on the blank solution and the resulting data are then treated statistically to obtain S_{bl} ($1.455\cdot10^{-8}$ A) and S_{bl} ($1.1014\cdot10^{-9}$ A). Finally, according to the following equation, the slope of calibration plot, m, (4.3 nA μM^{-1}) is used to convert S_m to C_m, which is defined as the detection limit, $C_m=(S_m-S_{bl})/m$. From the analysis of these data, we estimate that the limit of detection of H_2O_2 is of the order of 750 nM (Signal/Noise=3). The sensitivity and the lowest detection limit of the Ag/PMo12/PAni hybrid-modified electrode towards reduction of hydrogen peroxide were compared with the recently reported hybrid-modified electrodes [19, 21–23, 30, 35, 36] and are given in Table 1. As can be seen from Table 1, the present modified electrode

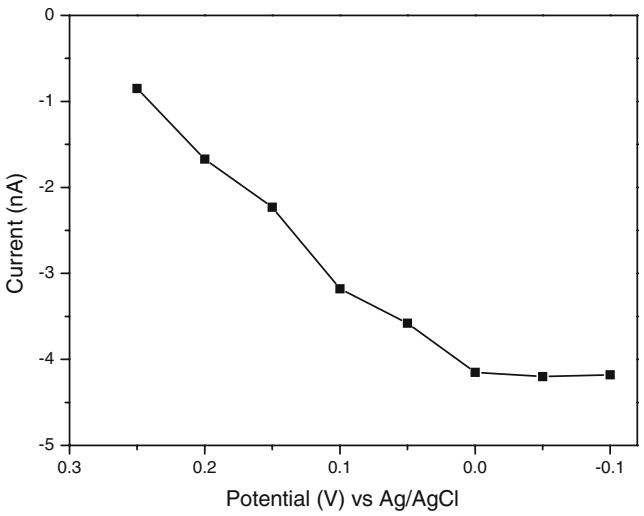

Fig. 7 Effect of applied potential on the amperometric sensing of 4 μM H_2O_2 at hybrid Ag/HPA/PAni-modified electrode in 1.0 M H_2SO_4 medium

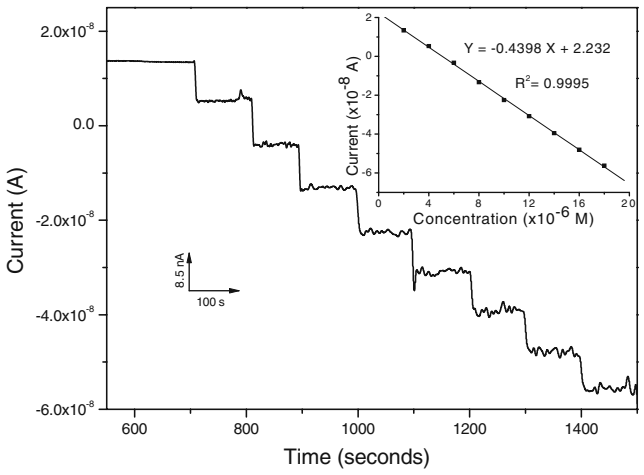

Fig. 8 Amperometric *i–t* curve for the determination of H_2O_2 at Ag/PMo12/PAni-modified electrode in 1.0 M H_2SO_4. Each addition increases the concentration of 2 μM of H_2O_2. E_{app}=0.0 V. The inset calibration plot shows effect of concentration on peak current towards reduction of hydrogen peroxide

Table 1 Comparison of different HPA hybrid-modified electrodes towards reduction of H_2O_2

Electrode	Modifier	Method	Potential	Sensitivity	Detection limit (M)	Reference
CPE	PMo12/PPy	CA	+0.180 V	1.1 μA mM^{-1}	$5{\cdot}10^{-5}$	[35]
GCE	PMo12–Au/PAni	CV	0.800 to −0.100 V	N\R	N\R	[30]
GCE	PMo12–Au/PPy	CV	0.700 to −0.100 V	N\R	N\R	[30]
GCE	P_2MoO_{18}/OMC	CA	0.0 V	0.7 μA mM^{-1}	$5.34{\cdot}10^{-5}$	[23]
CPE	α-$K_7P_2W_{17}VO_{62}$/Graphite/ Organoceramic	CA	+0.435 V	0.753 μA mM^{-1}	$4{\cdot}10^{-5}$	[21]
CPE	PMo12/pbpy	CV	0.800 to −0.200 V	N\R	N\R	[36]
CPE	$[PFeW_{11}O_{39}]^{4-}$/Silica gel	CA	0.0 V	0.183 nA μM^{-1}	$7.4{\cdot}10^{-6}$	[22]
Pt	PMo12/Solgel	CA	0.0 V	3.6 μA mM^{-1}	$7{\cdot}10^{-6}$	[19]
GCE	Ag/PMo12/PAni	CA	0.0 V	4.3 nA μM^{-1}	$7.5{\cdot}10^{-7}$	[This work]

N\R not reported, *CPE* carbon paste electrode

shows the lowest detection limit among the hybrid-modified electrodes for H_2O_2 (750 nM).

Finally, the operational stability of the Ag/PMo12/PAni-modified electrode was studied by repetitive cyclic voltammograms in 1.0 M H_2SO_4 solution. The good reproducibility of the cyclic voltammograms, indicates that the films was found to be extremely stable with in these potential limits with only loss of less than 10% in the overall electroactivity after 50 continuous potential cycles, which infer that Ag/PMo12/PAni-modified electrode may suitable for analytical applications.

Conclusions

The prepared hybrid Ag/PMo12/PAni material is successfully fabricated on the Glassy carbon electrode for the electrocatalytic reduction of hydrogen peroxide. The observed voltammetric results indicate that the charge transport in the modified electrode was fast and stable. Amperometric determination of H_2O_2 shows linear response over a range of 2 to 20 μM concentration with a sensitivity of 4.398 nA $\mu M^{-1}$and achieved lowest detection limit of 750 nM (Signal/Noise=3). Thus, the present work paves a way for the construction of hybrid Ag/PMo12/PAni-modified electrode and exploring its application in enzyme free concurrent electrochemical sensing of H_2O_2 which is a challenge task in the generation of nanoscale building blocks for electrochemical sensing.

Acknowledgement The authors thank DST, New Delhi and DEST, Australia for the sanction of INDIA-AUSTRALIAN strategic research fund (INT/AUS/P-1/07 dated 19th Sep 2007) for their collaborative research. In addition, authors thank DST, New Delhi for the sanction of FIST programme (SR/FST/CSI-066/2008, dated 12.01.2009). One of the authors, A. Manivel thanks CSIR, New Delhi for awarding Senior Research Fellowship.

References

1. Murray RW (ed) (1992) Molecular design of electrode surfaces. Wiley, New York
2. Finklea HO, Bard AJ, Rubinstein I (eds) (1996) Electro analytical chemistry, vol 19. Marcel Dekker, New York
3. Grundig B, Wittstock G, Rudd U, Strehlitz B (1995) J Electroanal Chem 395:143–157
4. Ramesh P, Sampath S (2000) Anal Chem 72:3369–3373
5. Zen JM, Senthil Kumar A, Tsai DM (2003) Electroanalysis 15:1073–1084
6. Sadakane M, Steckhan E (1998) Chem Rev 98:219
7. Liu M, Dong S (1995) Electrochim Acta 40:197–200
8. Muller A, Kogerler P, Kuhlmann C (1999) Chem Commun 1347
9. Lira-Cantu M, Gomez-Romero P (1998) Chem Mater 10:698–704
10. Vaillant J, Lira-Cantu M, Cuentas-Gallegos K, Casan-Pastor N, Gomez-Romero P (2006) Prog Solid Stat Chem 34:147–159
11. Kuhn A, Anson FC (1996) Langmuir 12:5481–5488
12. Carapuca HM, Balua MS, Fonseca AP, Cavaleiro AMV (2006) J Solid Stat Electrochem 10:10–17
13. Guanghan L, Xiaogang, Yanhua L, Shenlai Y (1999) Talanta 49:511–515
14. Keita B, Contant R, Abdeljalil E, Girard F, Nadjo L (2000) Electrochem Commun 2:295–300
15. Kulesza PJ, Chojak M, Karnicka K, Miecznikowski K, Palys B, Lewera A (2004) Chem Mater 16:4128–4134
16. Li S, Wang E, Tian C, Mao B, Song Y, Wang C, Xu L (2008) Mater Res Bulletin 43:2880–2886
17. Kulesza PJ, Skunik M, Baranowska B, Miecznikowski K, Chojak M, Karnicka K, Frackowiak E, Beguin F, Kuhn A, Delville MH, Starobrzynska B, Ernst AZ (2006) Electrochim Acta 51:2373–2379
18. Thangamuthu R, Wu YC, Chen SM (2009) Electroanalysis 21:1655–1658
19. Song W, Liu Y, Lu X, Xu H, Sun C (2000) Electrochim Acta 45:1639–1644
20. Wang B, Cheng L, Dong S (2001) J Electroanal Chem 516:17–22
21. Wang P, Wang X, Bi L, Zhu G (2000) J Electroanal Chem 495:51–56
22. Hamidi H, Shams E, Yadollahi B, Esfahani K (2009) Electrochim Acta 54:3495–3500
23. Zhou M, Guo L, Lin F, Liu H (2007) Anal Chim Acta 587:124–131
24. Guo W, Xu L, Xu B, Yang Y, Sun Z, Liu S (2009) J Appl Electrochem 39:647–652
25. Wang P, Wang X, Zhu G (2000) Electrochim Acta 46:637–641
26. Wang P, Wang X, Bi L, Zhu G (2000) Analyt 125:1291–1294
27. Wu QY, Wang HB, Yin CS, Meng GY (2001) Mater Lett 50:61–65

28. Gomez-Romero P (2001) Adv Mater 13:163–174
29. Kishore PS, Viswanathan B, Varatharajan TK (2008) Nanoscale Res Lett 3:14–20
30. Ernst AZ, Zoladek S, Wiaderek K, Cox JA, Kolary-Zurowska A, Miecznikowski K, Kulesza PJ (2008) Electrochim Acta 53:3924–3931
31. Keita B, Liu T, Nadjo L (2009) J Mat Chem 19:19–33
32. Lim SS, Park GI, Choi JS, Song IK, Lee WY (2002) Catal Today 74:299–307
33. Biju V, Sugathan N, Vrinda V, Salini SL (2008) J Mater Sci 43:1175–1179
34. Skoog DA, Holler FJ, Nieman TA (1998) Principles of Instrumental Analysis, 5th ed. Saunders College Publishing, Philadelphia
35. Wang X, Zhang H, Wang E, Han Z, Hu C (2004) Mater Lett 58:1661–1664
36. Lu J, Xiao FX, Shi LX, Cao R (2008) J Solid Stat Chem 181:313–318